Science and Technology Publishing (SCI & TECH)
ISSN: 2632-1017
Vol. 8 Issue 12, December - 2024

Determination Of The Effects Of Abrasive Wear Mechanisms On Aluminium Alloy (AA 6061) Under Operating Conditions Like Sliding Distance, Load And Sliding Speed

Edwin Edwin Ebiese[1]

Department of Mechanical and Aerospace Engineering,
University of Uyo, Uyo, Akwa Ibom State-Nigeria

Aniekan Offiong[2]

Department of Mechanical and Aerospace Engineering,
University of Uyo, Uyo, Akwa Ibom State-Nigeria

Idorenyin Etiese Markson[3]

Department of Mechanical and Aerospace Engineering,
University of Uyo, Uyo, Akwa Ibom State-Nigeria

***Abstract*— In this study, determination of the effects of abrasive wear mechanisms on aluminium alloy (AA 6061) under operating conditions like; sliding distance, load and sliding speed is presented. The aluminium alloy AA 6061 sample was prepared adapting the research process that included sectioning, abrasive wear test, wear measurement and chemical microanalysis using Scanning Electron Microscopy (SEM)/ Energy Dispersive X-Ray Spectroscopy (EDS or EDX).The insights were deduced from the results of the analysis are, one, the abrasive wear behaviour is dependent on the applied load, sliding distance and sliding speed mainly. Two, the wear is seen to increase at higher sliding speed and at higher applied load. It was seen at velocity of 10 m/s and 50 N load; the wear rate was higher in AA 6061and Abrasives Al2O3 and SiC. Three, the scanning electron microscope images of worn surfaces revealed cavities, pits, and cracks due to the plastic deformation and the delamination mechanism at higher loads (50 N). Finally, the abrasives; Al2O3 and SiC had lower wear rate and coefficient of friction when compared to the base alloy AA 6061. The knowledge acquired through this study is essential for the design and development of more durable and efficient automotive components.**.

Keywords — Abrasive Wear, Aluminium Alloy (AA 6061), Sliding Distance, Scanning Electron Microscopy (SEM)/ Energy Dispersive X-Ray Spectroscopy (EDS or EDX), Sliding Speed

1. Introduction

A lot of mechanical components and equipment are subjected to sliding contact in real time applications [1,2]. Such mechanical components that are frequently subjected to sliding wear include belt drives, valves, machinery guide ways, pumps as well as bearings and piston- cylinder arrangements [3,4]. Moreover, studies have shown that many failures in mechanical equipment occurred as a result of problems associated wear [5,6]. The widespread use of AA 6061 aluminium alloy in automotive components such as engine blocks, cylinder heads and gear boxes, has raised serious concerns about its tribological behaviour under operating conditions such as load, speed and temperature [7,8].

Abrasive wear, in particular, is significant mechanism that can lead to premature failure of these components, resulting in high cost of maintenance of automobile parts, reduced fuel efficiency and compromised safety [9]. High temperature affects the wear rate and mechanism of ceramic coatings in aerospace, equally, cycling loading affect wear rate and mechanisms of gears in turbines [10]. Therefore, understanding the effects of abrasive wear mechanism in mechanical components such as; pistons, engine blocks and gear boxes in automobiles under different operating conditions like; load, speed and temperature are important nucleus of this research.

Hence, this study is undertaken in order to fathom the effects of abrasive wear mechanism on aluminium alloy (AA 6061) of mechanical components under different operating conditions such as; (temperature, load and speed) and as well proffer solution in the industries by enhancing the wear resistance of AA 6061; to save cost, enhance service life of machine components and reliability of the machines. The knowledge acquired through this study will provide insights for the design and development of more durable and efficient automotive components.

2. Methodology

The aluminium alloy AA 6061 (with a sample shown in Figure 1) was prepared adapting the research process that included sectioning, abrasive wear test, wear measurement and chemical microanalysis using Scanning Electron Microscopy (SEM)/ Energy Dispersive X-Ray Spectroscopy (EDS or EDX).

Figure 1: Samples of AA 6061

2.1 Sectioning

Abrasive cut-off Wheels consist of abrasive grains (such as Aluminum Oxide or Silicon Carbide), bonded together with rubber or other materials in the form of a thin wheel was used in cutting the AA 6061 aluminium alloy into a manageable size and minimal heat generation was ensured to avoid altering the microstructure. Specifically, the cutoff wheels are first indexed starting from the hard to the soft which are denoted by "grade". As a rule of thumb, a hard bonded wheel was selected when sectioning soft stock of AA 6061. A reasonable amount of wheel pressure was applied so the abrasive grains to "bite" and remove the metal in fine chips.

2.2 Abrasive wear test

Two-body abrasive wear tests were performed on a pin-on-disc machine according to ASTM G-99 standards. To apply abrasive conditions during test, 600 grade SiCp emery paper was fixed on the rotating disc surface and the specimen was fixed in specimen holder. Before each test, each sample was cleaned by acetone and dried in air. The initial weight of the test specimen was recorded accurately using a digital electronic balance with a least count of 0.0001 grams. After fixing the emery paper on disc and the specimen pin in their respective positions, the normal load to the pin was applied by a pivoted loading lever with a string and pan assembly. The required loads were applied by placing known dead weights on the pan. In order to encounter fresh abrasives, the specimen was also moved against the parallel surface of the rotational steel disc.

Wear test was carried out by a pin-on-disc wear test apparatus at room temperature according to ASTM: G99 and normal applied loads of 10 N, 20 N, 30 N, 40 N and 50 N. The pins used were prepared from sintered AA 6061 and the pins were prepared in cylindrical shape which has 10 mm diameter and 55 mm length. It was ensured that the cylindrical pins do not have burr and sharp edges or sharp corners because it is known that such sharp corners in the pin can damage the surface of the disc when it is sliding. The surface roughness value of pins was measured and maintained as 0.8 µm (Ra) to get uniform wear result. Oil hardened non shrinkage (OHNS) steels with a hardness of 60 HRC were selected as the counterpart and its surface roughness also measured and recorded as 0.45 µm. The SiC paper with 600 grit sizes were used to smoothen the pins and counterpart surfaces aftwer which acetone was used to clean them. Again, after diamond paste and mechanical polishing machine such as ASTM: E3 were used for grinding the pins and counterpart surfaces, then fine polishing was conducted. At this point, perpendicularity check was conducted on the surface of the pins. At the same time, the flatness to seat with counterpart surface was also checked. At this point, the pin samples a prepared for use and they are arranged in slots that have been provided on the arm which is located above the rotating disc. The weights of the pins were measured before and after wear tests by using a sensitive electronic balance with an accuracy of 0.1 mg. The experiments were conducted under the normal load of 10 N, 20 N, 30 N, 40 N and 50 N at five different sliding velocities namely 2.0 m/s, 4.0 m/s, 6.0 m/s, 8.0 m/s and 10.0 m/s for sliding distances 20 m, 40 m, 60 m, 80 m and 100 m. The weight losses were calculated at every interval of sliding distances for different normal loads with respect to various sliding velocities. The friction coefficient was recorded during sliding by means of a XY plotter attached to the arm to which the pin was attached. The ratio of the weight and the density was used to determine the volume loss caused by the wear. Also, the ratio of volume loss to the sliding distance was used to determine the wear rate. The wear test process was repeated four times for each pin the average of the results obtained in the four instances was computed along with the error bars..

2.3 Wear measurement:

Wear rate was estimated by measuring the mass loss in the specimen after each test and mass loss, Δm in the specimen was obtained.

The mass loss was calculated by measuring the height loss (Δh) in each experiment, the area of cross section(A) of sample and the density (ρ) of the alloy by using the relation

$$\Delta m = \Delta h \times A \times \rho \quad (1)$$

Cares were taken after each test to avoid interaction of wear debris in the specimen.

Wear rate which relates to the mass loss (Δm) and sliding distance (L) was calculated using the expression,

$$W = \Delta m/L \quad (2)$$

For each pass in the wear test the friction force was measured and eventually the friction force was averaged from the value measured in all the passes. The average value of co-efficient of friction, μ of composite was calculated from the expression,

$$\mu = F_f / F_n \quad (3)$$

where F_f is the friction force and F_n is the total number of passes

2.4 Scanning Electron Microscopy (SEM)/ Energy Dispersive X-Ray Spectroscopy (EDS or EDX)

This equipment was used to perform chemical microanalysis in conjunction with scanning electron microscopy (SEM). This technique detected x-rays emitted by the specimen when bombardment by an electron beam. The primary purpose was characterizing the elemental composition of the analyzed volume. Scanning Electron Microscopy (SEM) was used to identify imperfections, cracks, or some foreign material inclusions on a surface. It was also used to study the microstructure along with finding the shape and sizes of smaller particles.

The microstructure examination process of the base AA 6061 alloy specimens was carried out via making the surface by grinding, polishing, etching, and then seen beneath an Optical microscope. The etching procedure was conducted on the polished surfaces via utilizing etchant reagent for the alloys of Al. Keller's reagent consists of 95 ml H_2O, 2.5 mL HNO_3, 1.5 ml HCl, and 1.0 ml HF. After that, the specimens were cleaned with water and alcohol and dried in the oven.

Scanning Electron Microscope (SEM) equipment provided with Energy Dispersive Spectroscopy (EDS) has studied the microstructure of SiC and Al_2O_3. Additionally, the alloy microstructures were performed to study the topography of the wear surfaces after the wear test

3. Results and discussion

3.1 Chemical Composition of the Aluminium Alloy AA 6061

The metal matrix selected for the study was based on Al-Si-Mg alloy system, designated by the American Aluminium Association as Al 6061. It offers a range of good mechanical properties and good corrosion resistance. The microstructure analysis of AA 6061 was conducted and the result is depicted in Figure 2. The chemical composition of Al 6061 alloy is shown in Figure 2.

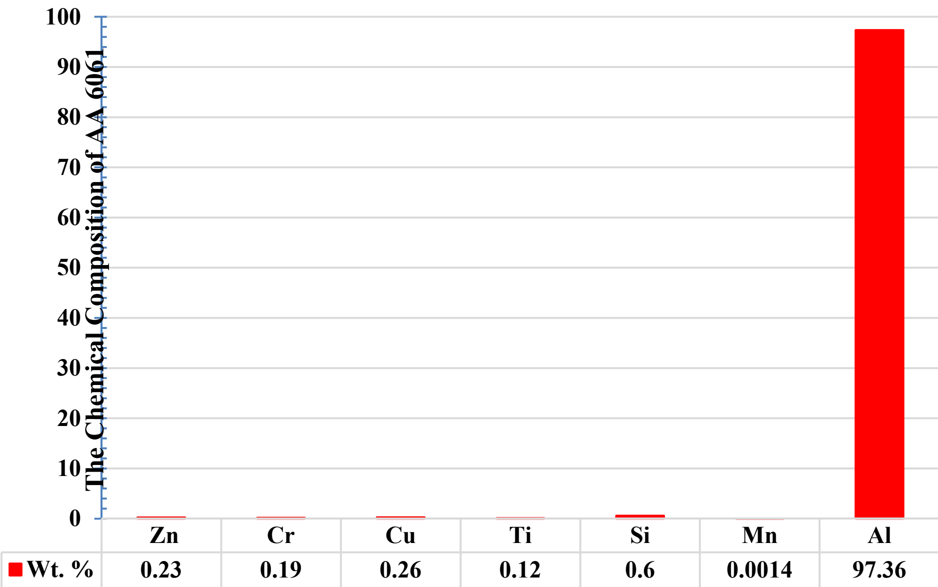

Figure 2 . The Chemical Composition of AA 6061

3.2 Scanning Electron Microscopy (SEM) Analysis of AA 6061 Aluminium Alloy

The microstructure of the AA 6061 when observed under scanning electron microscope (SEM) is presented in Figures 3. The microstructures of the aluminium composite sample showing reinforcement particles of SiC and Al_2O_3 which gave the fine and highly consistent grain structure is presented in Figure 4. The SEM micrographs in Figures 5 a and b view the microstructure of the base alloy and composite sample respectively, reinforced with hybrid addition ($SiC+Al_2O_3$) distribution of particles is homogenized totally. That is because the rotating tool gives adequate heat and circumferential force for dispersing the particles of (SiC) or (Al_2O_3) to become full in the broader region. The EDS analysis is presented in Figure 5 c for a composite reinforced with the hybrid addition of (SiC + Al2O3) particles. The SEM micrographs for the worn surface of AA 6061 alloy sample after wear test at 30 N load for 20 min; (a) at 200 µm (b) at 100 µm (c) at 50 µm are presented in Figure 6 while the SEM micrographs for worn surface AA 6061 alloy sample with SiC particles after wear test at 30 N load for 20 min ; (a) Secondary electron image at 200 µm (b) and (c) Backscatter images are presented in Figure 7.

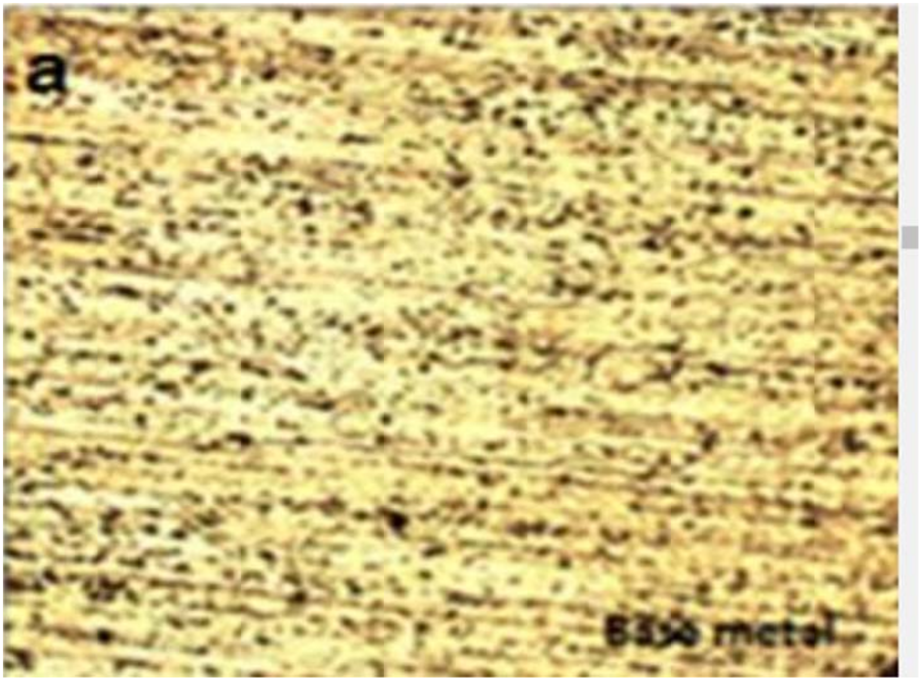

Figure 3: Scanning electron micrograph of AA 6061

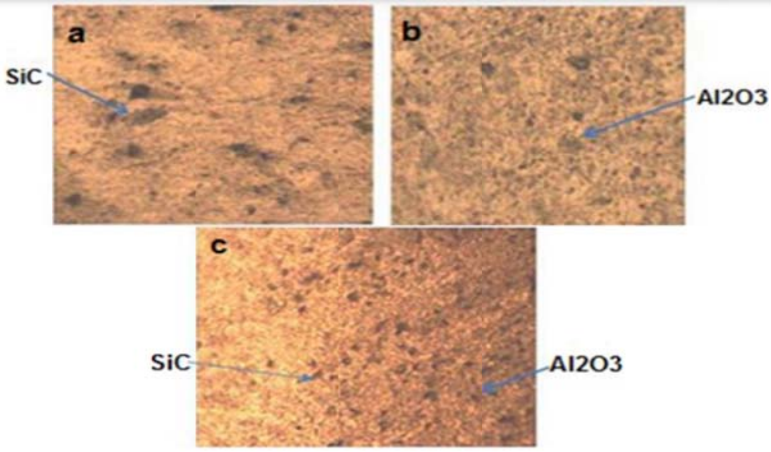

Figure 4.: The microstructures of composite sample showing reinforcement particles distributed in stir zone at optimum conditions at 100x; (a) sample with SiC particles, (b) sample with Al_2O_3 particles and (c)sample with hybrid (SiC+ Al_2O_3) particles.

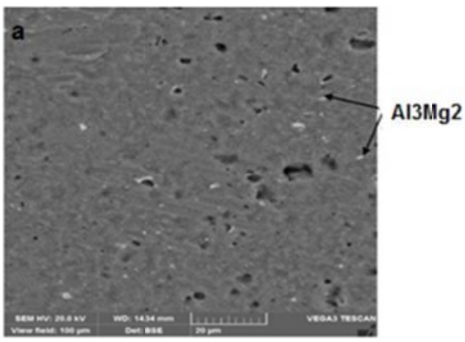

(a)

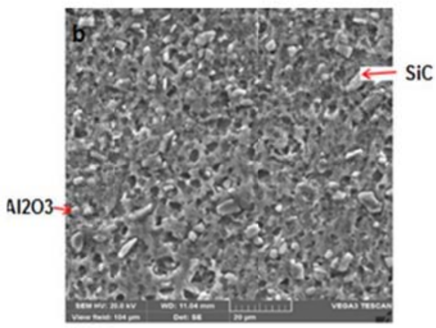

(b)

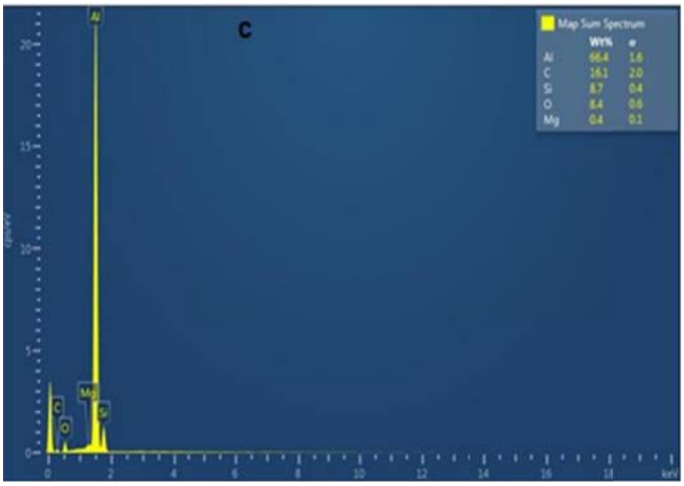

(c)

Figure 5 (a) SEM micrograph of AA 6061 alloy at 20 µm (b) SEM Micrograph of composite sample reinforced with hybrid SiC+Al_2O_3) particles (c) EDS analysis.

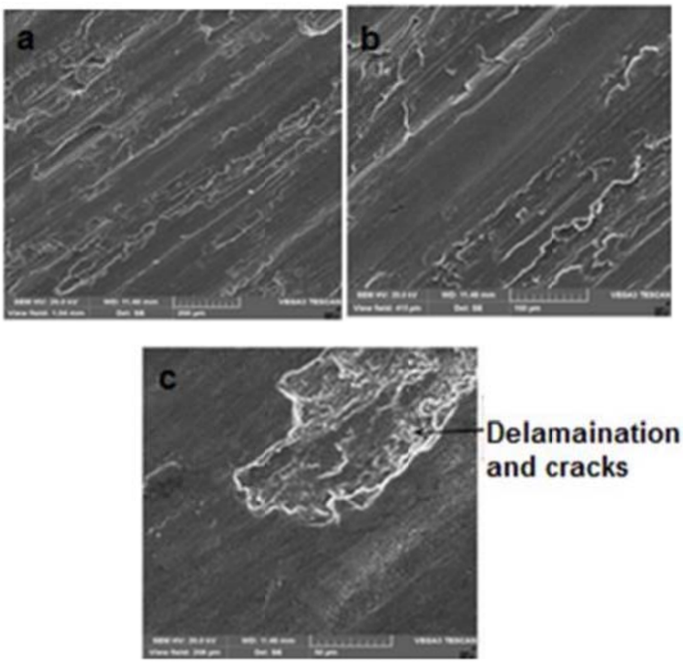

Figure 6: SEM micrographs for the worn surface of AA 6061 alloy sample after wear test at 30 N load for 20 min; (a) at 200 µm (b) at 100 µm (c) at 50 µm.

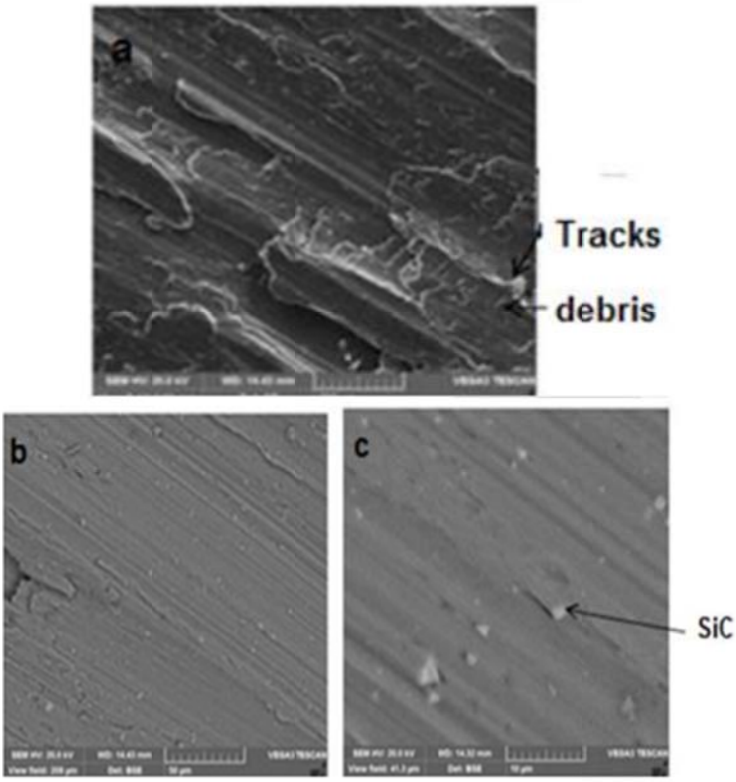

Figure 7: SEM micrographs for worn surface AA 6061 alloy sample with SiC particles after wear test at 30 N load for 20 min ; (a) Secondary electron image at 200 µm (b) and (c) Backscatter images.

3.3 Wear Test Results

The wear rate was measured by the procedure of the loss of weight for the base materials. The weight loss and wear rate increase with the loads rising as well as the speed and sliding distance. The plan of experiments was developed aiming at the influence of applied load (L), sliding speed (S) and sliding distance (D) with the two-body abrasive wear of the Al alloy AA 6061. By conducting the experiments, the abrasive wear results for various combinations of parameters were obtained and shown in Tables 1, Tables 2 and Tables 3. From the results in Tables 1 to Tables1, it was observed that increase in applied load and sliding distance increases the wear rate, also decrease in velocity decreases the wear rate. Again, Table 4 depicts coefficient of friction for aluminium alloy AA 6061, Al_2O_3 and SiC.

Table 1: Applied load on the wear rates for aluminium alloy AA 6061

Load (N)	Wear rates (m^3/m)
10.0	0.0014
20.0	0.0025
30.0	0.0029
40.0	0.0035
50.0	0.0054

Table 2: Sliding distance on the wear rate of aluminium alloy AA 6061

Sliding distance (m)	Wear rates (m^3/m)
20.0	0.00030
40.0	0.00038
60.0	0.00050
80.0	0.00075
100.0	0.00150

Table 3: Sliding velocity on the wear rates for aluminium alloy AA 6061

Sliding velocity (m/s)	Wear rates (m^3/m)
2.0	0.000013
4.0	0.000045
6.0	0.000090
8.0	0.000110
10.0	0.000275

Table 4: Coefficient of friction for aluminium alloy AA 6061, Al_2O_3 and SiC

Load (N)	Coefficient of friction		
	1(AA6061)	2 (Al_2O_3)	3(SiC)
10	0.172	0.195	0.135
20	0.268	0.200	0.181
30	0.342	0.226	0.215
40	0.395	0.316	0.293
50	0.415	0.323	0.298

3.4 Effect of Applied Load, Sliding Distances and Sliding Velocities on Wear Rate.

The wear rates for the AA 6061 as function of load, sliding distance and sliding velocities were shown in Figure 8, Figure 9 and Figure 10. From Figure 8, the wear rate increased linearly with increasing sliding distance under applied load because of abrasion wear exhibited for low sliding velocity 2 m/s. The presence of abrasive wear in low velocity has been reported by previous studies also (Shanthi et al., 2010). Also, from Figure 8, the rate of increase of wear rate from 20 to 100 m sliding distance was high at high load (50 N) compared to low loads (5 N and 10 N). At high sliding velocity (10.0 m/s), the rate of increase of wear rate from 20 to 100 m sliding distance was comparatively low (Figure 13) for all normal applied loads for both Al_2O_3 and SiC because of severe oxidation. From Figure 12, Figure 13 and Figure 14, it is evident from the results that the higher wear rate was observed at the higher normal load (50 N) and at high sliding velocity (10.0 m/s).

Main effect plots for abrasive wear volume loss of Al 6061 alloy matrix, Al_2O_3 and SiC reinforced Al alloy composites are represented in the Figure 12, Figure 13 and Figure 14. It is clear from Figure 12, Figure 13 and Figure 14 that sliding distance has the greatest effect under the optimal testing conditions followed by the applied load. As the sliding distance increases wear rate also increases. This is because as the sliding distance increases a greater number of abrasives comes into contact. It is further inferred from the Figures that the influence of applied load on wear behaviour is also significant. This can be attributed to an increase in penetration ability of the fractured particles with increase in load. The influence of sliding speed shows a slight effect and it contributes to a lesser extent compared to the sliding distance and applied load. As the sliding speed increases the wear rate decreases. It is clear from Tables 5, Tables 6 and Tables 7 as well as from Figure 12, Figure 13 and Figure 14 that sliding distance has more contribution on abrasive wear followed by applied load as reported in past studies (Sahin, 2005). This is because the abrasive particles were rigidly fixed on emery paper and they did not move freely or change their position against the specimen during sliding.

So, the load was effectively transferred from the abrasive to the specimen surface. Penetration ability of SiCp abrasive particles in emery paper into the specimen tested increased due to lower hardness of Al alloy. As the sliding distance increased, a higher number of cycles was required to complete the test and more asperities came in contact with specimen surface. Under the influence of applied load, the projected sharp SiC abrasive particles were effectively transferred to the specimen surface and they were either plastically deformed or remained in elastic contact. This resulted in increasing cutting efficiency of the abrasive particles. So that the material removal rate increased for specimen tested. Under this condition the deformation of few SiCp and composite were adhered to specimen. As the sliding speed increased, the material removed less, because increase of speed decreased the removal rate.

As shown in Tables 5, Tables 6 and Tables 7, it was noticed that the rates of wear of the friction stir processing composite specimens strengthened by SiC and Al_2O_3 particles are lesser than the processing base material, and that is as a result of the strengthening (SiC) and (Al_2O_3) particles which work as the particle of reinforcement of the Al alloy (AA6061) that distributed into the matrix of Al. The addition of strengthening particles reduces the rate of wear since the hard particles being dragged out from the composite specimen by the pin through the procedure of wear developed on the steel disc and worked as an obstacle.

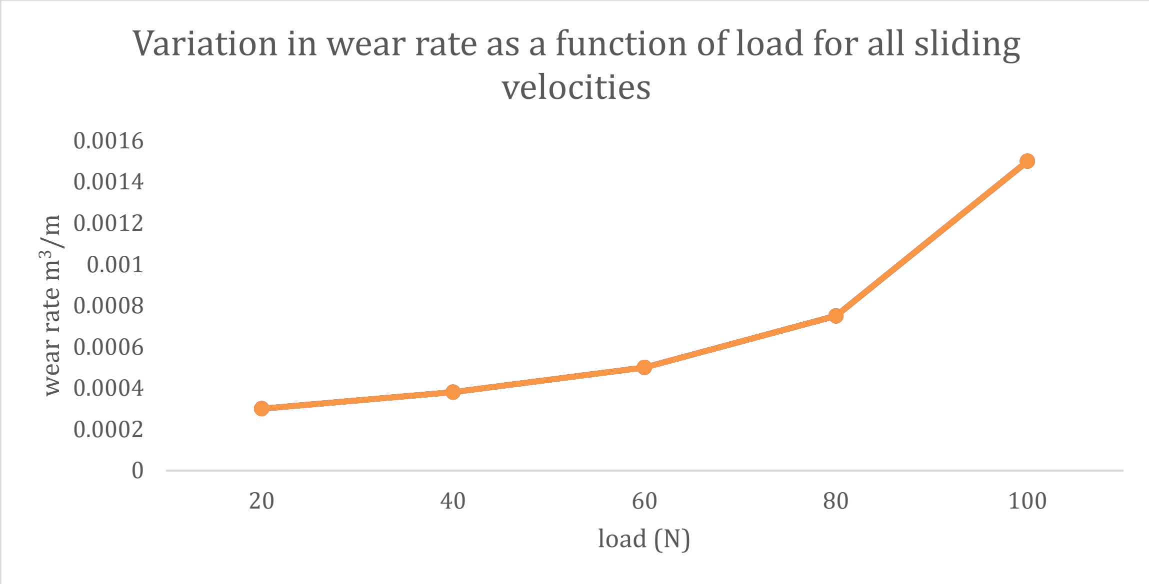

Figure 8: Variation in wear rate as a function of loading for all sliding velocities

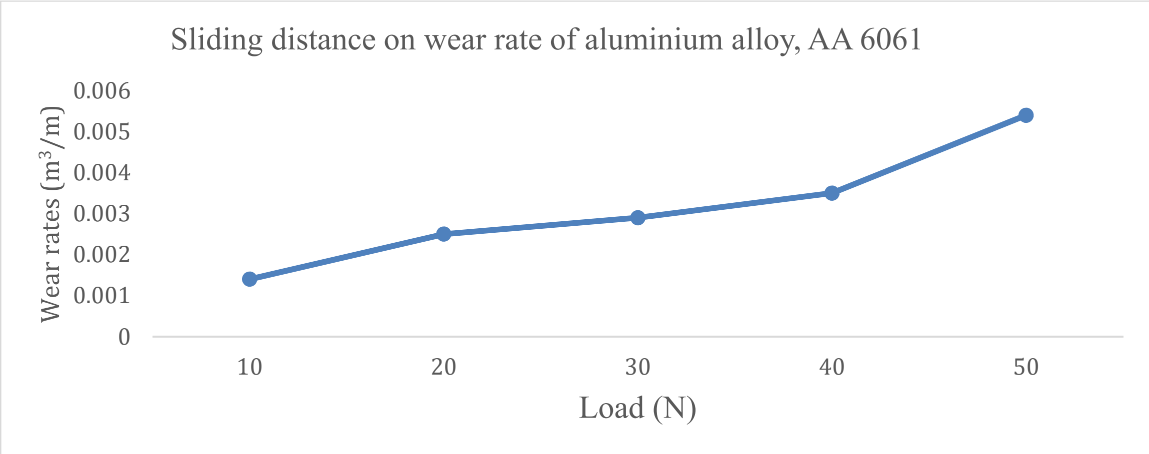

Figure 9: Sliding distance on wear rate of AA 6061

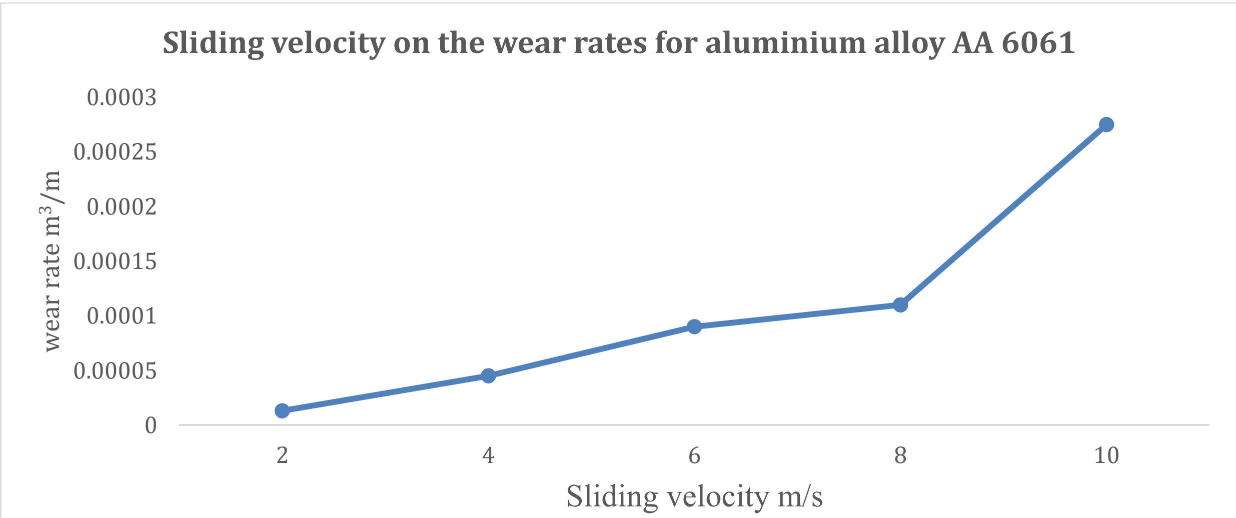

Figure 10: Sliding velocity on wear rate of AA 6061

Table 5: Sliding distance values of aluminium alloy AA 6061, Al_2O_3 and SiC

Sliding distance (m)	Wear rates (m^3/m)			
	AA 6061	Al_2O_3	SiC	
20.0	0.00030	0.00021	0.00013	
40.0	0.00038	0.00028	0.00019	
60.0	0.00050	0.00040	0.00025	
80.0	0.00075	0.00065	0.00045	
100.0	0.00150	0.00128	0.00112	

Table 6: Sliding velocity values of aluminium alloy AA 6061, Al_2O_3 and SiC

Sliding velocity (m/s)	Wear rates (m^3/m)			
	AA 6061	**Al_2O_3**	**SiC**	
2.0	0.000013	0.000010	0.000008	
4.0	0.000045	0.000035	0.000025	
6.0	0.000090	0.000080	0.000070	
8.0	0.000110	0.000107	0.000102	
10.0	0.000275	0.000255	0.000225	

Table 7: Applied load values of aluminium alloy AA 6061, Al_2O_3 and SiC

Load (N)	Wear rates (m^3/m)			
	AA 6061	**Al_2O_3**	**SiC**	
10.0	0.0014	0.0010	0.0008	
20.0	0.0025	0.0015	0.0011	
30.0	0.0029	0.0019	0.0014	
40.0	0.0035	0.0025	0.0017	
50.0	0.0054	0.0036	0.0024	

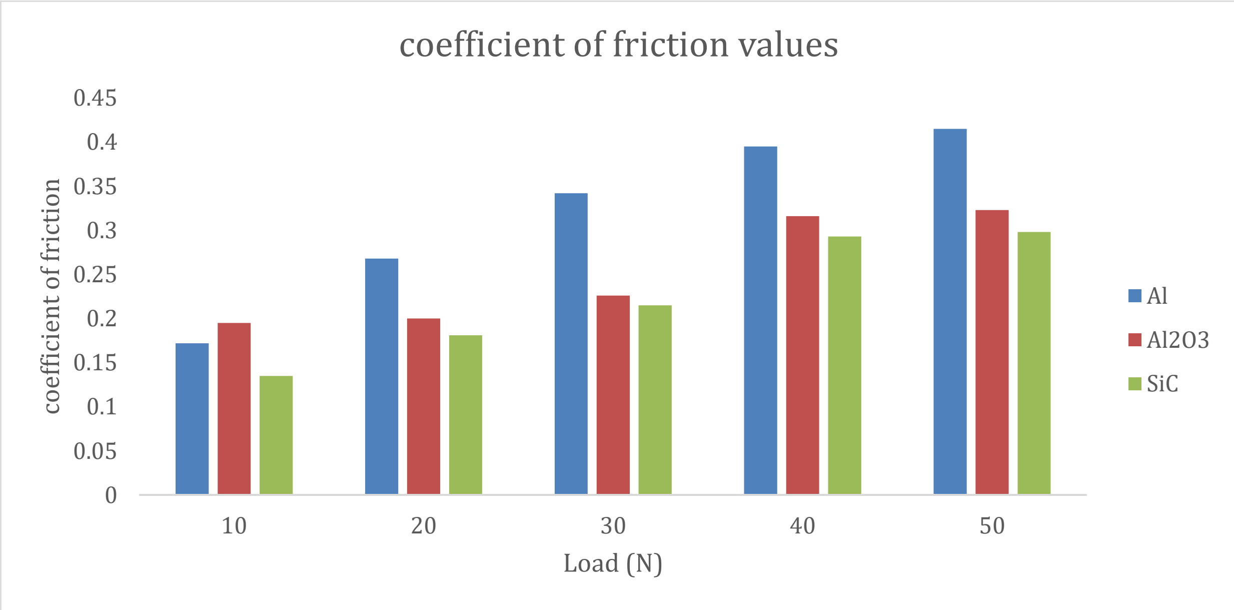

Figure 11: Coefficient of friction values with different composites at all applying load condition

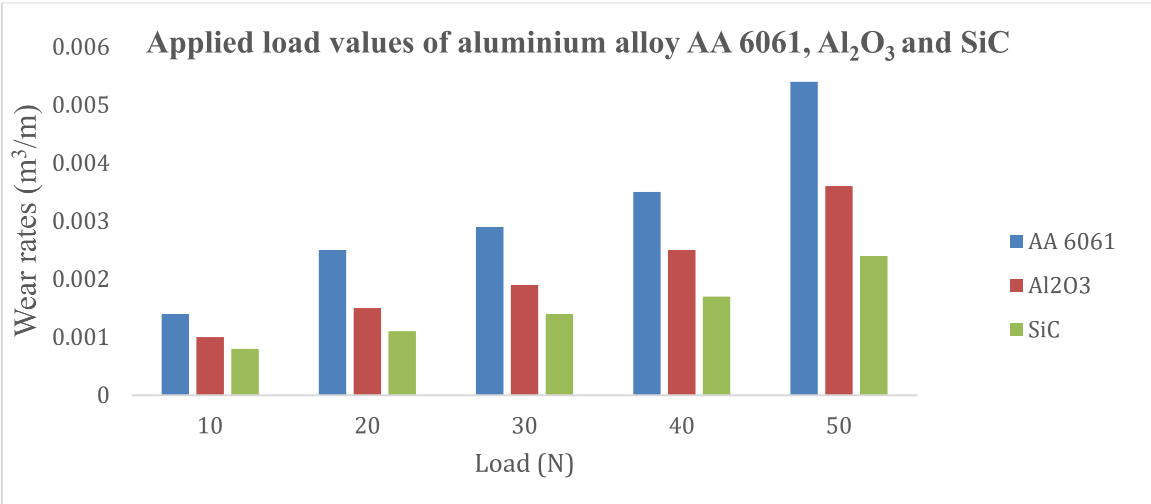

Figure 12: Wear rate of different composites at all applying load condition

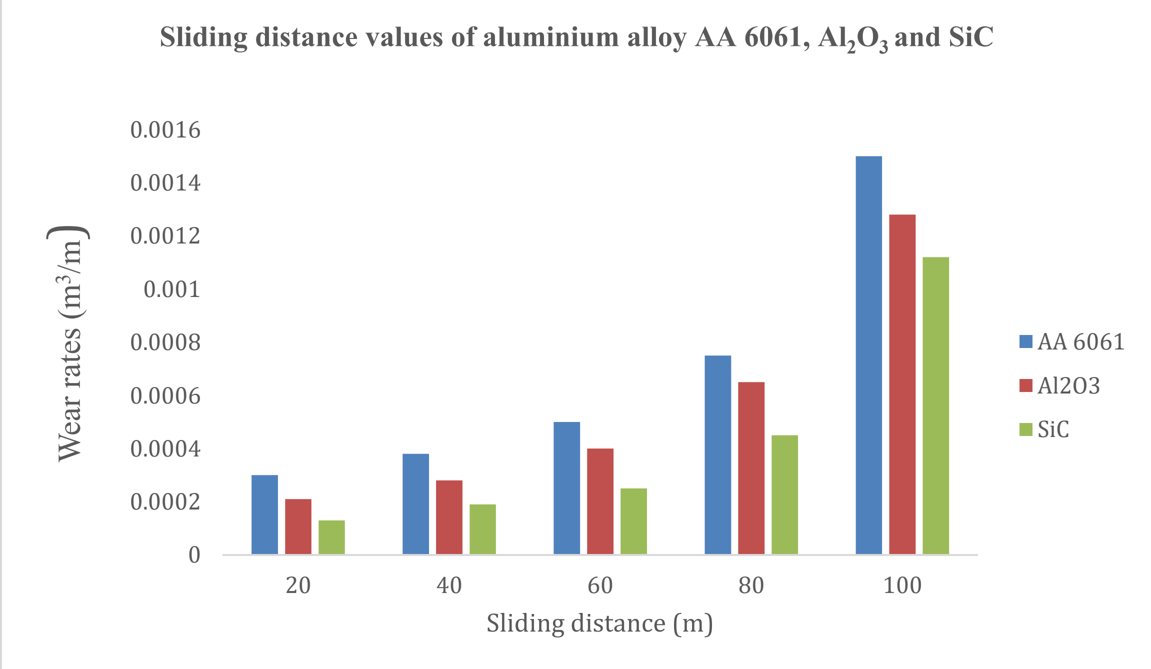

Figure 13: Wear rate of different composites at all sliding distance

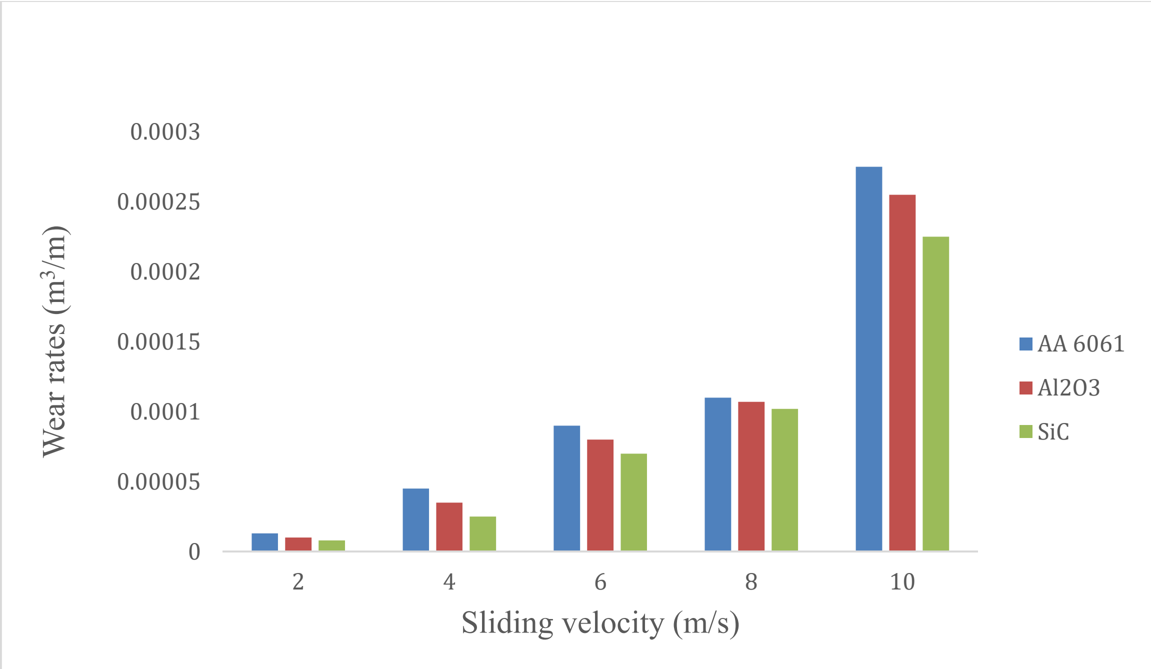

Figure 14: Wear rate of different composites at all sliding velocity

3.5 Characterization of Worn Surfaces

It is noticed from SEM images that the tracks or wear paths and grooves of wear rise in the friction stir processed specimen, and the cracks alongside the track raise the worn-out surface (Abbass and Sharhan, 2023). Fundamentally comprising incompletely uneven pits as well as longitudinal grooves. One can conclude from the study of microstructure that abrasive wear mainly occurs with certain adhesive wear traces. With the loads increasing, the wear lines width is augmented and causes grooves with the remark of big and small cracks propagated upon the specimen's surface, where such cracks convergence being developed with reinforcement particles SiC and/or Al_2O_3 is better in the resistance to wear than the specimens at the whole exerted loads. That's owing to the particles' role of (SiC+Al+ Al_2O_3) in refining the grains of the matrix of Al alloy as well as the hardness of the high particles of (SiC+ Al_2O_3). Figure 6 presents the scanning electron microscope (SEM) images of the worn surface. The deep and broad grooves and tracks take place in the friction processed specimen. That's owing to the intensive removal of material and the plastic deformation, which resulted in work hardening of the metal surface and formation of cracks that raise the debris of wear upon the worn surfaces. Sareh *et al*. (2016) showed that the wear debris could act as abrasive particles between two surfaces of specimen and rotating disk. Also, they were concluded from SEM micrographs of the worn surface of unreinforced alloy, the predominate wear mechanism was adhesive wear. While in the Aluminum-SiCp, the wear mechanism changed from adhesive to abrasive. This was due to the existence of ceramic particles that spread uniformly upon the worn surface, which does not permit the wear and severe material removal. It means that reducing the wear debris formation on the surface can improve the wear resistance of the composite. Such outcomes are similar to the Mohamed and Muna (2014) investigated the conduct of the wear of aluminium alloy fabricated by powder metallurgy.

4. Conclusion

The objective of this study was to determine the effects of abrasive wear mechanisms on aluminium alloy (AA 6061) under operating conditions like; sliding distance, load and sliding speed. Investigating and evaluating the effects of load, sliding distance and velocity on AA 6061 alloy due to abrasive wear mechanism. The relationship between abrasive wear rate, applied load, sliding distance and sliding speed in automotive components such as; piston, engine blocks and gear boxes was analyzed. Wear tests and Scanning Electron Microscope (SEM) were conducted to ascertain the effects of abrasive wear mechanism on mechanical components under different operating conditions.

References

1. Kloch, K. T., Kozak, P., & Mlyniec, A. (2021). A review and perspectives on predicting the performance and durability of electrical contacts in automotive applications. *Engineering Failure Analysis*, *121*, 105143.
2. Marian, M., & Tremmel, S. (2021). Current trends and applications of machine learning in tribology—A review. *Lubricants*, *9*(9), 86.
3. Hemanth, G., & Suresha, B. (2021). Hybrid and electric vehicle tribology: a review. *Surface Topography: Metrology and Properties*, *9*(4), 043001.
4. Litwin, W. (2023). *Water-Lubricated Journal Bearings: Marine Applications, Design, and Operational Problems and Solutions*. Elsevier.
5. Bourassa, D., Gauthier, F., & Abdul-Nour, G. (2016). Equipment failures and their contribution to industrial incidents and accidents in the manufacturing industry. *International journal of occupational safety and ergonomics*, *22*(1), 131-141.
6. Odeyar, P., Apel, D. B., Hall, R., Zon, B., & Skrzypkowski, K. (2022). A review of reliability and fault analysis methods for heavy equipment and their components used in mining. *Energies*, *15*(17), 6263.
7. Ghazi, A. K., Taieh, N. K., & Khudhur, S. K. (2022). Investigation of Dry Tribo-Behavior of Aluminum Alloy AA6061/Al 2 O 3/Graphite Composites Synthesized by Stir Casting Technique. *Journal of Composite & Advanced Materials/Revue des Composites et des Matériaux Avancés*, *32*(5).
8. Wu, X., & Zhang, W. (2024). A review on aluminum matrix composites' characteristics and applications for automotive sector. *Heliyon*.
9. Zhang, W., & Xu, J. (2022). Advanced lightweight materials for Automobiles: A review. *Materials & Design*, *221*, 110994.
10. Karmakar, D. P., Muvvala, G., & Nath, A. K. (2021). High-temperature abrasive wear characteristics of H13 steel modified by laser remelting and cladded with Stellite 6 and Stellite 6/30% WC. *Surface and Coatings Technology*, *422*, 127498.